Nanoscale

The role of surface functionalization in quantum dot-based photocatalytic CO_2 reduction: balancing efficiency and stability

Journal:	*Nanoscale*
Manuscript ID	NR-ART-12-2023-006177.R1
Article Type:	Paper
Date Submitted by the Author:	26-Jan-2024
Complete List of Authors:	Hernandez, Frida; Amherst College, Chemistry Yang, Maggie; Amherst College, Chemistry Nagelj, Nejc; Amherst College, Chemistry Lee, Autumn; Amherst College, Chemistry Noh, Hasun; Amherst College, Chemistry Hur, Kyle; Amherst College, Chemistry Fu, Xinyu; Amherst College, Chemistry Savoie, Caleb; Amherst College, Chemistry Schwartzberg, Adam; Lawrence Berkeley National Laboratory, Molecular Foundry Olshansky, Jacob; Amherst College, Chemistry

The role of surface functionalization in quantum dot-based photocatalytic CO_2 reduction: balancing efficiency and stability

Frida Hernandez,[1] Maggie Yang,[1] Nejc Nagelj,[1] Autumn Y. Lee,[1] Hasun Noh,[1] Kyle P. Hur,[1] Xinyu Fu,[1] Caleb J. Savoie,[1] Adam M. Schwartzberg,[2] Jacob H. Olshansky[1]*

[1]Department of Chemistry, Amherst College, Amherst, MA 01002, USA

[2]The Molecular Foundry, Lawrence Berkeley National Laboratory, Berkeley, CA 94720, USA

Email: *jolshansky@amherst.edu

Electronic Supplementary Information (ESI) available: Additional photocatalysis data and details on calculations, additional transient absorption data and analysis.

Abstract

Photocatalytic CO_2 reduction offers a promising strategy to produce hydrocarbons without reliance on fossil fuels. Visible light-absorbing colloidal nanomaterials composed of earth-abundant metals suspended in aqueous media are particularly attractive owing to their low-cost, ease of separation, and highly modifiable surfaces. The current study explores such a system by employing water-soluble ZnSe quantum dots and a Co-based molecular catalyst. Water solubilization of the quantum dots is achieved with either carboxylate (3-mercaptopropionic acid) or ammonium (2-aminoethanethiol) functionalized ligands to produce nanoparticles with either negatively or positively-charged surfaces. Photocatalysis experiments are performed to compare the effectiveness of these two surface functionalization strategies on CO_2 reduction and ultrafast spectroscopy is used to reveal the underlying photoexcited charge dynamics. We find that the positively-charged quantum dots can support sub-picosecond electron transfer to the carboxylate-based molecular catalyst and also produce >30% selectivity for CO and >170 mmol CO g_{ZnSe}^{-1}. However, aggregation reduces activity in approximately one day. In contrast, the negatively-charged quantum dots exhibit >10 ps electron transfer and substantially lower CO selectivity, but they are colloidally stable for days. These results highlight the importance of the quantum dot-catalyst interaction for CO_2 reduction. Furthermore, multi-dentate catalyst molecules create a trade-off between photocatalytic efficiency from strong interactions and deleterious aggregation of quantum dot – catalyst assemblies.

Introduction

Fundamental research on the conversion of CO_2 to hydrocarbon fuels and value-added carbon compounds is necessary to advance new technologies that reduce reliance on fossil fuels and remove excess atmospheric CO_2.[1,2] Ideally, such technologies would rely on either renewable electricity or direct sunlight.[3,4] Direct photocatalysis is particularly attractive since it can be implemented without intermediate electrical systems, and may be more economically viable than photoelectrochemical systems.[5] Semiconducting nanoparticles, or quantum dots (QDs), have recently emerged as promising sensitizers for photocatalytic CO_2 reduction.[4,6,7] QDs are robust visible light absorbers that offer tunable redox energies *via* composition[8–11] and size control,[12–14] and can support significant chemical variety in surface functionalization.[15–17] Furthermore, there is extensive literature using QDs for other photocatalytic conversions, including proton reduction to hydrogen,[18–23] C-C coupling,[24–28] alcohol oxidation,[29] and nitrogen fixation.[30] A theme of this body of work is the critical role that the surface plays in dictating catalysis,[15] thus motivating our exploration of the role of surface functionalization in photocatalytic CO_2 reduction using QDs.

A variety of metrics must be considered when choosing a specific QD composition for photocatalysis. For example, semiconductors with smaller bandgaps can absorb more of the visible spectrum, but offer less driving force for redox reactions.[4] To access photocatalytic CO_2 reduction to CO semiconductors must possess a conduction band energy greater than approximately -4.0 vs. vacuum or -0.77 vs. SCE.[3] Promising visible light-absorbing semiconducting materials that have been employed for CO_2 reduction (bulk conduction band position vs. vacuum) include: CdS (-3.9 V),[31–36] ZnSe (-3.4 V),[26,31,37–41] $CuInS_2$ (-3.0 V),[42–46] and lead halide perovskites (-4.0 – -3.0V).[47,48] Environmental concerns may motivate researchers to use materials that do not contain toxic heavy metals such as Pb and Cd. We have chosen to focus our attention on ZnSe QDs since they are

heavy-metal free, provide clear size-dependent excitonic features, and exhibit minimal defect absorption.[49,50]

A molecular catalyst is typically used in QD-based photocatalytic CO_2 reduction schemes to improve selectivity and yield. A large literature exists for molecular and heterogeneous CO_2 reduction catalysis,[3,51,52] providing a library of potential catalysts that can be combined with the light-absorbing QDs. We are particularly drawn to cobalt tetraphenylporphyrin (Co-TPP) catalysts,[53] since they use an earth-abundant metal and are associated with the most productive QD-based CO_2 systems for both ZnSe[38] and $CuInS_2$.[42] Prior work demonstrates the importance of attaching catalysts to the surface of QDs. Kuehnel *et al* explored a series of nickel terpyridine catalysts coupled with CdS QDs and found that the anchoring group affected CO selectivity and production rate.[34] Huang *et al* found a >3x enhancement in CO production when covalently linking a Re catalyst to $CuInS_2$ QDs compared to physically mixing the catalyst and QD.[45] We have therefore chosen a Co-TPP catalyst functionalized with carboxylic acids that can bind to QD surfaces.

Surface modification of as-synthesized QDs is nearly always required to prepare photocatalytic systems. Typically, native hydrophobic ligands are exchanged for hydrophilic ligands that impart solubility in common CO_2 reduction solvents such as DMF, DMSO, and water. Mercaptopropionic acid (MPA) is a commonly used ligand as its thiol group binds strongly to the surface of metal chalcogenide quantum dots[54] and its carboxylate group imparts solubility. MPA has been used in photocatalytic CO_2 reduction schemes using CdS,[32,33] $CuInS_2$,[43,45] and ZnSe[26,37] QDs. This work can also be informed by the larger literature of mercaptocarboxylate-QDs used for hydrogen evolution (HER).[19,21–23] For example, Wilker *et al* explored a series of mercaptocarboxylate ligands with different numbers of carbons (n) on CdS nanorods used for

photocatalytic HER. They found that carbon chain length significantly altered hydrogen production rates. Nanorods with mercaptoacetic acid (n = 2) were ~4x more productive than nanorods with MPA (n = 3), and longer chains were significantly worse.[22] Short ligands are therefore critical for enabling efficient charge extraction and subsequent catalysis using QDs; however, trade-offs could exist when aiming to suppress HER relative to CO_2 reduction.

Surface functionalization strategies that do not involve carboxylates have also been employed. Work by Reisner and colleagues found that ligand-stripped CdS QDs, stabilized by BF_4^- ions, produce two orders of magnitude more hydrogen than MPA-functionalized CdS QDs.[23] The Reisner group has also used BF_4-stabilized ZnSe QDs for photocatalytic CO_2 reduction in multiple studies,[38–41] producing as much as 79.7 mmol CO g_{ZnSe}^{-1}.[38] Surface functionalization with ammonium moieties has produced particularly promising results. Feng *et al* compared CO production using CdS QDs functionalized with MPA, BF_4, and 4-mercaptopyridinium, producing 3 μmol, 0.19 mmol, and 20.3 mmol CO g^{-1} h^{-1}, respectively.[35] The 4-mercaptopyridinium QDs were therefore far superior and, in total, produced ~450 mmol CO g_{CdS}^{-1}. The Weiss group found similarly high levels of CO production using 2-aminoethanethiol (AET) as a capping ligand on $CuInS_2$ QDs (~850 mmol CO g_{QD}^{-1}).[42] These results were rationalized by the affinity between CO_2 and amines.

The prevalence of studies employing carboxylate-functionalized QDs (typically MPA) coupled with the promise of ammonium-functionalized QDs motivates our current work to directly compare these two surface-functionalization strategies for CO_2 reduction. Notably, there are no prior reports that make such a comparison using QD-molecular systems that only differ in the terminal functional group of the ligand. The current works directly compares carboxylate (MPA) and ammonium (AET) functionalized QDs. We have performed CO_2 reduction experiments with

MPA and AET functionalized ZnSe QDs and a Co-TPP catalyst. We show that AET QDs initially produce significantly more CO than MPA QDs with a CO selectivity ~4x greater than MPA QDs. However, the AET QDs deactivate after approximately one day, while the MPA QDs continue to produce H_2 and CO for up to three days. We use both steady state absorption and ultrafast transient absorption spectroscopy to rationalize these observations. In particular, AET QDs facilitate rapid (sub-ps) electron transfer to the catalyst, while electron transfer in the MPA QDs is slower than the intrinsic QD relaxation (tens of ps). However, AET QDs form aggregates, which likely lead to their accelerated deactivation. Both of these observations can be understood as a consequence of stronger catalyst-QD interactions in the AET QDs. This strong interaction and associated sub-picosecond electron transfer allows the AET ZnSe QDs to achieve up to 170 mmol CO g_{ZnSe}^{-1} in water, the highest value reported for photocatalytic CO_2 reduction with ZnSe QDs. Furthermore, this work highlights the importance of considering ligand-catalyst interactions.

Results and Discussion

Prior to describing the CO_2 reduction experiments, we have provided details on the synthesis and relevant energetics of the ZnSe QDs and the Co-TPP catalyst. Stearate-capped ZnSe QDs were synthesized in accordance with prior literature,[49] and subsequently ligand-exchanged with either AET or MPA to achieve water solubilization. QD size and concentrations were determined using UV-Vis absorption and standard sizing curves.[50] All QDs used for photocatalysis experiments had a diameter of d = 3.6 nm and a bandgap of 3.1 eV. The Co-TPP catalyst was synthesized in accordance with prior literature.[55] The relevant energetics for all components of the photocatalytic system are provided in Scheme 1. Oxidation potentials for sacrificial hole scavengers, sodium ascorbate (NaAsc)[56] and triethanolamine (TEOA),[57] are positioned such that there is a large driving force (> 1 V) for hole extraction. The Co-TPP catalyst has been shown to

be chemically reduced from Co(III)-TPP to Co(II)-TPP in the presence of hole scavengers such as NaAsc.[53] The relevant step for initiating CO_2 capture and reduction is therefore photoexcited electron transfer from the QD to Co(II)-TPP, generating Co(I)-TPP with a reduction potential of -0.92 V vs. SCE.[53] Reduction potentials for both CO_2 to CO and HER are accessible by the reduced catalyst. These two reactions are therefore in competition, and are independently monitored in the present study.

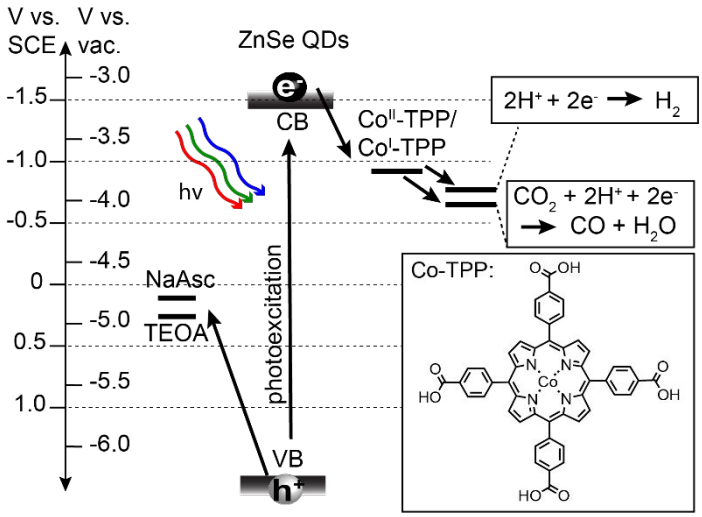

Scheme 1. Relevant processes and energetics for photocatalytic CO_2 reduction using ZnSe QDs. Oxidation potentials for sacrificial hole scavengers, sodium ascorbate (NaAsc) and triethanolamine (TEOA), are shown as well as reduction potentials for the Co-TPP catalyst and relevant reactions (CO_2 reduction and HER).

Photocatalysis experiments were performed on the QD systems using a home-built photoreactor and reaction products were monitored by gas chromatography (GC). In a typical experiment, aqueous samples (2 mL) were prepared containing 0.4 μM ZnSe QD, 0.4 μM Co-TPP, and a hole scavenger (25-400 mM). We used a 1:1 ratio of QDs to catalyst based on prior work with the same catalyst.[42] Samples were saturated with an atmosphere of CO_2 and placed in a six-well photoreactor equipped with 400 nm LEDs. The head space was sampled periodically with an air tight syringe and directly injected into the GC (See Table S1 for complete data). Two metrics are primarily used to assess photocatalytic efficiency: turnover number and selectivity. The total

amount of CO (or H_2) produced relative to the amount of catalyst (or QD) is the turnover number (TON). The ratio of CO produced relative to total gaseous products (CO and H_2) gives the CO selectivity (See SI for details of calculations). Control experiments verified that all components were necessary to produce substantial CO (light, CO_2, hole scavenger, QD, and catalyst). The QDs and light alone (with or without hole scavenger), however, were sufficient in producing substantial H_2 (see Table S2). Reaction mixture pH was recorded after equilibration to be in the range of 6.4 - 6.5, which we ascribe to a carbonic acid and bicarbonate buffer created by dissolved CO_2.

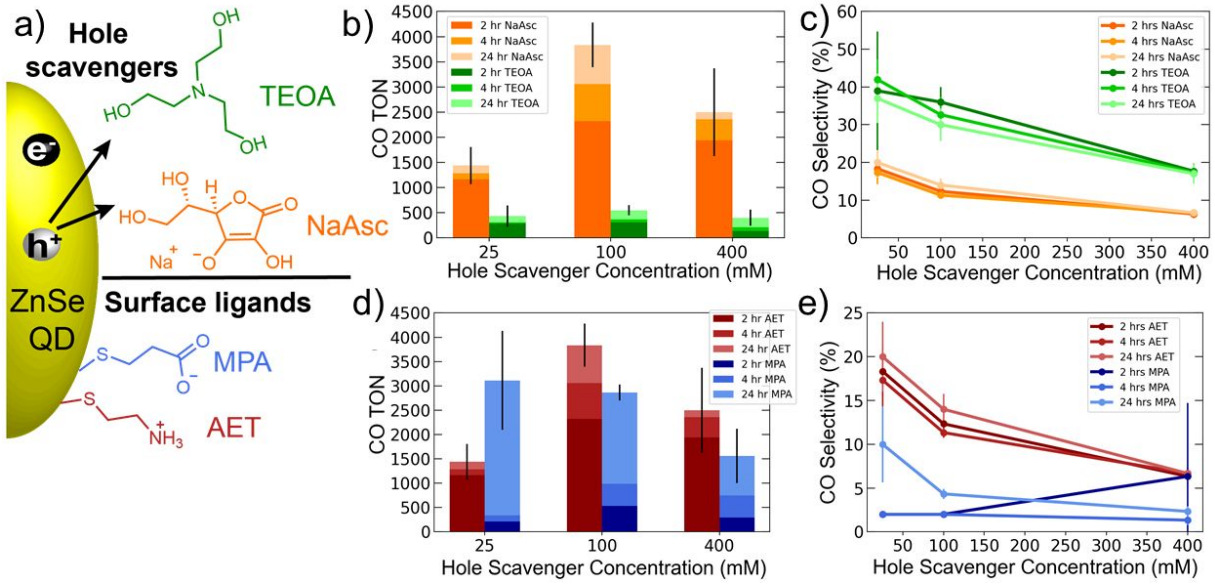

Figure 1. Results of photocatalysis experiments with varying hole scavenger concentrations and identities. a) Schematic of hole scavengers and surface ligands. b-c) CO TON and selectivity for AET QDs and both TEOA and NaAsc hole scavengers at different concentrations. d-e) CO TON and selectivity for both AET and MPA QDs with varying NaAsc concentration. Photocatalysis experiments were performed in triplicate on 2.0 mL aqueous solutions of 0.4 μM ZnSe QDs and 0.4 μM Co-TPP, irradiated with 400 nm LEDs.

Initial experiments explored the role of the hole scavenger. Figure 1a shows the two hole scavengers, NaAsc and TEOA, as well as the surface ligands used: MPA and AET. AET QDs were used for comparing the hole scavengers. The results of these experiments are shown in Figure 1b-c and show a significant suppression of HER by TEOA, which yields a CO selectivity >40%.

However, CO production was also significantly lower with TEOA. We therefore decided to use NaAsc as the hole scavenger for all subsequent experiments. Another important trend revealed by this data is that increasing hole scavenger concentration reduces selectivity. A careful look at the specific CO and H_2 TONs shows that this trend is driven by enhanced HER at higher hole scavenger concentrations. This suggests that accelerating hole extraction predominantly benefits HER, while CO_2 reduction is rate limited by other factors, likely related to the catalyst.

A comparison of AET and MPA QDs is presented in Figure 1d-e. These data show that AET QDs produce CO more selectively and initially in greater quantities than MPA QDs across a range of hole scavenger concentrations. This observation is consistent with prior literature suggesting that ammonium-functionalized QDs are better suited for CO_2 reduction owing to their affinity for CO_2,[42] but the role of catalyst binding must also be considered (see below).

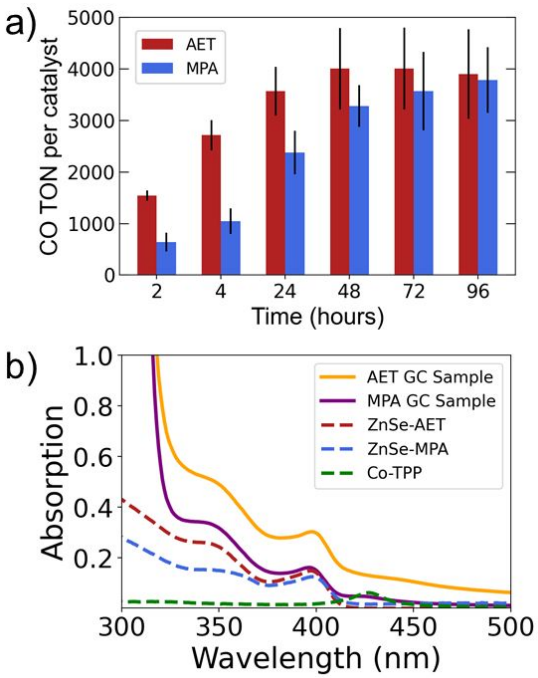

Figure 2. a) Longer experiments comparing AET and MPA QDs. b) UV-Vis spectra of reaction mixtures (GC samples) overlain with ligand-functionalized QDs and catalyst at identical concentrations alone in solution (dashed lineds). Photocatalysis experiments were performed in triplicate on 2.0 mL aqueous solutions of 0.4 μM ZnSe QDs, 0.4 μM Co-TPP, and 100 mM NaAsc. Samples were irradiated with 400 nm LEDs.

The results comparing AET and MPA QDs (Figure 1d) suggest that the two systems have differing long-term behavior. Specifically, AET QDs initially produce more CO, but after 24 hours the MPA QDs are able to produce comparable amounts of CO. We therefore performed 4-day experiments (Figure 2a) that reveal the same trend with greater clarity: the AET QDs produce >2x more CO at four hours, but CO production slows by the second day while MPA QDs continue to produce CO throughout the third day. We hypothesize that the more rapid deactivation of the AET QDs may be a result of aggregation. To verify this hypothesis, UV-Vis absorption spectra of AET and MPA ZnSe QDs in pure water and in the reaction mixture (at identical concentrations) are performed (Figure 2b). There is a notable increase in light scattering for the AET QDs that is induced either by the addition of NaAsc or Co-TPP.

We believe that the aggregation observed in AET QD samples is driven by electrostratic interactions between the positively-charged AET QDs and the negatively charged NaAsc or tetracarboxylate Co-TPP. This hypothesis is supported by work from the Weiss group employing MPA-capped QDs and tetramethylammonium functionalized Fe-TPP catalysts for CO_2 reduction.[43] In their work, the negatively-charged QDs formed aggregates with the positively-charged catalyst. Furthermore, they found that larger aggregates produced less CO. In our work, with a negatively-charge catalyst, the positively-charged AET QDs aggregate over time while the negatively-charged MPA QDs remain colloidally stable. The aggregated AET QDs reduce available active sites for CO_2 reduction leading to deactivation. However, the electrostatic interaction between AET QDs and both hole scavengers and catalysts likely drives their higher initial CO production as compared to MPA QDs.

To better understand and compare the specific interactions and charge dynamics that occur between AET or MPA QDs and the catalyst or hole scavenger, we utilized femtosecond transient

absorption spectroscopy. This technique allows us to chart the pathways and timescales for photoexcited charge movement, thus providing insights on chemical interactions and the photophysical processes that underly photocatalysis. Transient absorption experiments were performed on AET and MPA ZnSe QDs with and without Co-TPP and NaAsc (eight samples total). All samples exhibited similar features in the transient spectra. Example spectra for AET QDs with neither catalyst nor NaAsc are shown in Figure 3a (see Figures S6-7 for all spectra). These spectra contain two notable features: 1) broad photo-induced absorption (450 – 600 nm) that has previously been assigned to surface-trapped holes,[41] but may also be a result of trapped electrons[58] and 2) a transient excitonic bleach at 400 nm that is ascribed to electron population in the conduction band.[41,58] We cannot distinguish any spectral signatures associated with the Co-TPP, likely because it is substantially broadened in the presence of QDs (Figure 2b).

Transient dynamics were extracted from the data by fitting kinetics at 500 nm (trapped carriers) and 400 nm (conduction band electrons). The 500 nm kinetics for all samples were quite similar, with a ~500 fs rise-time and a bi-exponential decay with time constants of ~100-200 ps and 5-15 ns (see Figure S7 and Table S3). This indicates that the spectrally accessible trapped carriers are minimally impacted by the addition of catalyst or NaAsc. The excitonic bleach kinetics at 400 nm show clear differences between the AET and MPA QDs (Figure 3b-c, Table 1). Kinetics of photoexcited electrons in AET QDs are significantly impacted by either the addition of catalyst or hole scavenger, while MPA QDs exhibit similar kinetics under all conditions.

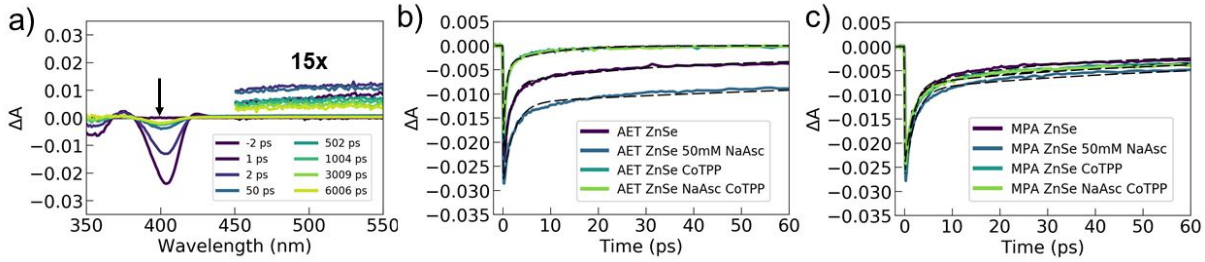

Figure 3. Transient absorption spectroscopy of ZnSe QDs with (and without) the Co-TPP catalyst or NaAsc hole scavenger. a) Transient spectra of AET ZnSe QDs at varying times after laser excitation. An excitonic bleach feature is observed at 400 nm and broad photo-induced absorption at longer wavelengths (multiplied by 15 for clarity). Kinetic traces of the excitonic bleach feature (400 nm) are shown for (b) AET and (c) MPA QDs. All samples were excited at 350 nm and had 5-6 μM QDs. Co-TPP was included in a 1:1 ratio to the QDs, and NaAsc (50 mM). Bi-exponential fits, convoluted with an instrument response function, are overlaid (dashed black lines).

The transient data can help us rationalize the differences between the performance of the MPA and AET QDs. The excitonic data for the MPA QDs indicate that electron transfer to Co-TPP proceeds *via* electron traps, and on a slower time scale than exciton relaxation (1 – 50 ps). In contrast, photoexcited electrons in AET QDs are rapidly extracted when Co-TPP is included. In these samples, the majority of the excitonic bleach decays with a time constant of ~500 fs. We ascribe this time constant to electron transfer to Co-TPP, and its rapidity indicates that Co-TPP is bound to the AET QD surface. Furthermore, the addition of NaAsc to AET QDs (without Co-TPP) slows down recovery of the bleach, indicating that electrons are residing in the QD conduction band longer. This is likely a result of efficient hole sequestration by NaAsc, which reduces the availability of holes with which electrons can recombine. It is puzzling that there is no concomitant change in the photoinduced absorption feature ascribed to trapped carriers, but this may be a result of spectrally silent charge carriers playing a role. Overall, these data unambiguously demonstrate that AET QDs support more efficient electron and hole extraction than their MPA QD counterparts. Notably, photoexcited electron transfer from AET QDs to Co-TPP occurs on a sub-picosecond timescale. We posit that the favorable charge extraction kinetics are a result of

electrostatic interactions that attract the negatively-charged NaAsc and Co-TPP to the surface of the positively-charged AET QDs.

Table 1. Exponential fitting parameters for 400 nm kinetic traces. All times reported in picoseconds.

	A_1	τ_1 (error)	A_2	τ_2 (error)	A_{inf}
AET ZnSe	-0.017	1.39 (0.09)	-0.00056	33 (4)	-0.0024
AET ZnSe 50 mM NaAsc	-0.017	2.29 (0.17)	-0.0063	109 (12)	-0.0056
AET ZnSe CoTPP	-0.021	0.55 (0.03)	-0.0041	7.9 (0.9)	0
AET ZnSe NaAsc CoTPP	-0.017	0.60 (0.04)	-0.0038	10 (1)	0
MPA ZnSe	-0.021	1.47 (0.10)	-0.0067	26 (3)	-0.0017
MPA ZnSe 50 mM NaAsc	-0.019	2.08 (0.15)	-0.0064	61 (7)	-0.0026
MPA ZnSe CoTPP	-0.019	1.82 (0.13)	-0.0063	45 (5)	-0.0018
MPA ZnSe NaAsc CoTPP	-0.017	1.81 (0.13)	-0.0058	45 (5)	-0.0023

Data were fit to bi-exponential decay functions of the form $\Delta A(t) = A_1 e^{-\frac{t}{\tau_1}} + A_2 e^{-\frac{t}{\tau_2}} + A_{inf}$ and included convolution of an instrument response function of ~130 fs.[59]

With a better understanding of the relevant surface interactions and charge dynamics for our system in hand, we aimed to optimize the system for CO production by varying the catalyst number per QD. Since QDs can accommodate multiple molecules on their surface, we explored ratios ranging from 0.25 to 30 Co-TPP per AET QD (Figure 4). It is important to recall that the work presented in Figures 1-3 employed a 1:1 ratio. The highest CO TONs per catalyst were achieved at low catalyst concentrations, but increasing catalyst concentration was found to markedly increase selectivity, up to 30%. At high catalyst loadings, we were able to obtain the highest values for mmol CO produced per gram of QD among ZnSe QD-based photocatalytic CO_2 reduction systems.

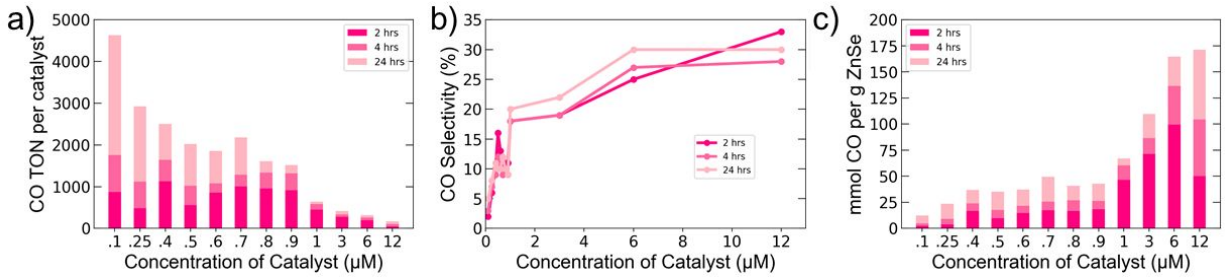

Figure 4. Effect of varying Co-TPP concentration on CO_2 reduction. a) CO TON per catalyst, (b) CO selectivity, and (c) mmol CO produced per gram of ZnSe QDs. Photocatalysis experiments were performed on 2.0 mL aqueous solutions of 0.4 μM ZnSe QDs and 50 mM NaAsc. Samples were irradiated with 400 nm LEDs.

Conclusions

This paper explores the interplay between QD surface functionalization and catalyst chemistry through photocatalysis experiments and ultrafast spectroscopy. Positively-charged QDs were prepared through surface functionalization with 2-aminoethanethiol (AET) while negatively-charged QDs were prepared using 3-mercaptopropionic acid (MPA). These QDs were mixed with a carboxylic acid-functionalized CO_2 reduction catalyst, expected to be negatively charged at neutral pH. We found that the positively charged AET QDs support rapid (sub picosecond) photoexcited electron transfer to the catalyst and produced CO in higher quantities and with significantly higher selectivity than the MPA QDs, which supported >10 ps electron transfer. Electrostatic interactions between catalysts' carboxylate groups and positively-charged AET QDs can explain these observations. Such interactions are not possible for the MPA QDs. Furthermore, after approximately one day, the AET QDs deactivate while the MPA QDs remain active for CO_2 reduction. We believe this to be a result of electrostatic-driven QD-catalyst-QD aggregation. Taken as a whole, there is a trade-off between catalytic efficiency and stability when using catalysts with multiple binding groups. A strong catalyst-QD interaction leads to more efficient CO_2 reduction, but also deleterious aggregation.

The importance of the chemical interaction between the catalyst and the QD surface suggests a variety of potential future experiments. We first observe that the suitability of a specific

surface functionalization for a specific photocatalytic reaction is highly dependent on the catalyst chemistry. One strategy to disentangle these effects would be to compare our current system with ammonium-functionalized catalysts and MPA QDs. Furthermore, the potential for QD aggregation must be carefully managed. Altering the ionic strength of the solution or using catalysts functionalized with only one binding group are two strategies that may mitigate the effects of aggregation.

Materials and Methods

Synthesis and Sample Preparation

Chemicals: Zinc stearate ($ZnSt_2$, tech.), Selenium powder (Se, 99.99% trace metals basis), 4,4',4'',4'''–(Porphine-5,10,15,20-tetrayl)tetrakis(benzoic acid) (TPP, dye content 75%), dimethyl sulfoxide (DMSO, reagent 99.5%), sodium *l*-ascorbate (NaAsc, crystalline 98%), triethanolamine (TEOA, 99.0% (GC)), 2-aminoethanethiol (AET, 95%), and hydrochloric acid (HCl, reagent 37%) were purchased from Sigma-Aldrich. 1-octadecene (ODE, tech., 90%) was purchased from Acros Organics. Cobaltous chloride hexahydrate and 3-mercaptopropionic acid (MPA, 99%) were purchased from Fisher Scientific Chemicals. Solvents used were toluene, acetone, methanol, MilliQ water, and chloroform.

ZnSe QD Synthesis: The synthesis of Zinc Selenide (ZnSe) QDs was adapted from Banski *et al* and has been used in previous studies.[41,49,60] Zinc stearate (0.4 mmol), selenium powder (0.4 mmol), and 26 mL of ODE were measured into a 100 mL three-neck round bottomed flask with a stir rod and degassed at room temperature for an hour. The solution was then heated to 295 °C under N_2. After one hour, the solution was rapidly cooled to room temperature by blowing air onto the flask. To precipitate the QDs, 30 mL of acetone was added to the flask. For cleaning, the QDs were washed with acetone and centrifuged three times with additional acetone to remove ODE.

The QDs were then redispersed in toluene (9 mL) and precipitated with the addition of acetone followed by centrifugation. The QDs were redispersed in toluene, cleaned with acetone and methanol, and centrifuged an additional three times. Following cleaning, the QDs were resuspended in 5 mL of toluene and transferred into a glove box for storage. Reported ZnSe QD sizes are calculated using UV-Vis spectra and standard sizing curves.[50]

Co-TPP Synthesis: The synthesis of Co-TPP was adapted from Nakazono *et al*.[55] $CoCl_2 \bullet 6H_2O$ (90 mg, 6 mmol), and TPP (90 mg, 1 mmol) were weighed into a 50 mL three-neck round bottomed flask and dissolved in 25 mL of DMSO. This solution was refluxed for 24 hours. The flask was then cooled to room temperature and 1 M HCl (75 mL) was added to the solution to precipitate the crude product as a purple solid. This solid was collected by filtration, washed with water, and dried under vacuum. Finally, the solid was redissolved in 0.1 M NaOH (20 mL) and 1 M HCl (40 mL), causing deposition of the product as a dark purple solid which was collected by filtration and dried under vacuum. Aqueous solutions were prepared using dilute NaOH, and concentrations determined from previously reported extinction coefficients (155,000 M^{-1} cm^{-1}).[42,53]

Ligand Exchange with MPA: 80 μL of 3-mercaptopropionic acid, 3 mL of chloroform, 350 μL of a 65 μM ZnSe QD stock solution, and 2 mL of MilliQ water were combined and agitated in a centrifuge tube and 500 μL of 0.25 M NaOH was added. This solution was sonicated and then left to stir overnight. The following day the solution was centrifuged, separating the chloroform and water layers. These layers were individually removed, characterized, and stored. The presence of MPA ZnSe QDs in the water layer was confirmed through UV-Vis spectroscopy.

Ligand Exchange with AET: 50 mg of 2-aminoethanethiol hydrochloride, 3 mL of chloroform, 350 μL of a 65 μM ZnSe QD stock solution, and 2 mL of MilliQ water were combined and agitated in a centrifuge tube. This solution was sonicated and centrifuged, separating the chloroform and

water layers. These layers were individually removed, characterized, and stored. The presence of AET ZnSe QDs in the water layer was confirmed through UV-Vis spectroscopy.

Photocatalysis Experiments: All samples were prepared to have 2.0 mL of total volume with varying concentrations of the ZnSe QDs (usually 0.4 μM), Co-TPP (0.1 – 12 μM), and hole scavengers (25 – 400 mM) in MilliQ water. All samples were prepared in 24 mL vials equipped with rubber septa and stir bars. Sealed vials were purged (using a needle) with N_2 for 5 minutes and bubbled with CO_2 for 10 minutes before being placed in the photoreactor. When running simultaneous experiments, samples were placed in the photoreactor with 10-minute delays to keep timing consistent when performing gas sampling. Head-space sampling of the vials was performed by removing 0.5 mL of gas with a 1.0 mL air tight syringe and needle, and directly injecting into the gas chromatograph.

Instrumentation

UV-Vis Absorption: Spectra were collected using an Agilent Technologies Cary 60 UV-Vis spectrophotometer. The ZnSe QDs, Co-TPP, and hole scavenger solutions were dispersed in MilliQ water for a total volume of 2 mL for absorption measurements (to be consistent with reaction mixtures). The spectra were measured in quartz cuvettes with 1 cm path lengths.

Photoreactor: The photoreactor consists of 6 LEDs (LEDSupply UV-A High Power LED Star, #A007-UV400-65) and associated lenses (Carclo, #10193) mounted on a heat sink (MakersHEATSINK SLIM) and connected in series. The LEDs are powered with a constant current source (Mean Well APC 25-700) set to 700 mA. A 3D-printed container allows six vials to be suspended over the LEDs and was equipped with a 12 V cooling fan. The temperature in all

six vials was tested during long-term operation (24 hours) and was stable at 35 ºC. The power density at the sample position was measured to be ~200-250 mW cm^{-2}.

Gas Chromatography (GC): An SRI Instruments Multiple Gas Analyzer #5 GC equipped with two columns (a 6' molecular sieves, 5 Å, column and a 2-meter HAYSEP-D column) and two detectors (a thermal conductivity difference detector and a flame-ionization detector with a methanizer). All experiments were performed with a direct injection procedure onto the 6' mol-sieves column and chromatograms collected for each of the detectors. A calibration gas containing 1.00% each of H_2, CO, CO_2, CH_4 in N_2 was used each day of experiments to calibrate gas concentrations. The moles of CO and H_2 produced by photocatalysis were calculated assuming 22 mL of gaseous volume in the reaction vials. The high concentration of CO_2 present in the GC injections necessitated daily baking of the column at 250 ºC to remove trapped CO_2.

Femtosecond Transient Absorption Spectroscopy: An ultrafast transient absorption system with a tunable pump and white-light probe was used to measure the ZnSe QD exciton bleach and trapped carrier populations as a function of pump-probe delay time. The laser system consists of a regeneratively amplified Ti:sapphire oscillator (Coherent Libra), which delivers 4-mJ pulse energies centered at 800 nm with a 1-kHz repetition rate. The pulse duration of the amplified pulse is approximately 100 fs. The laser output is split by an optical wedge to produce the pump and probe beams and the pump beam wavelength is tuned using a coherent OPerA optical parametric amplifier. The probe beam is focused onto a sapphire plate to generate a white-light continuum probe. The transient absorption spectra are collected with a commercial absorption spectrometer (Helios, Ultrafast Systems LLC). The temporal behavior is monitored by increasing the path length of the probe pulse and delaying it with respect to the pump pulse with a linear translation stage (minimum step size 16 fs). The pump wavelength was maintained at 350 nm with a pulse power

between 100 nJ to 300 nJ. Residual pump light was filtered out of the collection optics using cross polarization.

Author Contributions

F.H., M.Y., N.N., and A.L. contributed equally to this work. F.H. performed data collection, curation, and visualization of photocatalysis data and wrote portions of the materials and methods. M.Y. synthesized ZnSe QDs, developed the methodology for photocatalysis data collection and curation, and collected photocatalysis data. N.N. synthesized the Co-TPP catalyst and developed the methodology for gas chromatography experiments. .A.L. performed data curation, developed methodology, and prepared visualizations for transient absorption data and wrote relevant portions of the materials and methods. A.L., K.H., H.N., and X.F. assisted in photocatalysis data collection. C.S. and A.L. prepared ZnSe QDs used in transient absorption experiments. A.S. supervised transient absorption data collection and wrote relevant portions of the materials and methods. J.O. supervised, conceptualized, and obtained funding for this project and wrote the original draft of the manuscript. All authors reviewed and edited the manuscript.

Conflicts of Interest

There are no conflicts to declare.

Acknowledgments

Acknowledgment is made to the Donors of Petroleum Research Fund, administered by the American Chemical Society, for partial support of this research, under Grant Number 61874-UNI4. Work at the Molecular Foundry was supported by the Office of Science, Office of Basic Energy Sciences, of the U.S. Department of Energy under Contract No. DE-AC02-05CH11231.

References

(1) Artz, J.; Müller, T. E.; Thenert, K.; Kleinekorte, J.; Meys, R.; Sternberg, A.; Bardow, A.; Leitner, W. Sustainable Conversion of Carbon Dioxide: An Integrated Review of Catalysis and Life Cycle Assessment. *Chem. Rev.* **2018**, *118* (2), 434–504. https://doi.org/10.1021/acs.chemrev.7b00435.

(2) Kong, T.; Jiang, Y.; Xiong, Y. Photocatalytic CO2 Conversion: What Can We Learn from Conventional COx Hydrogenation? *Chem. Soc. Rev.* **2020**, *49* (18), 6579–6591. https://doi.org/10.1039/C9CS00920E.

(3) Dalle, K. E.; Warnan, J.; Leung, J. J.; Reuillard, B.; Karmel, I. S.; Reisner, E. Electro- and Solar-Driven Fuel Synthesis with First Row Transition Metal Complexes. *Chem. Rev.* **2019**, *119* (4), 2752–2875. https://doi.org/10.1021/acs.chemrev.8b00392.

(4) Stolarczyk, J. K.; Bhattacharyya, S.; Polavarapu, L.; Feldmann, J. Challenges and Prospects in Solar Water Splitting and CO2 Reduction with Inorganic and Hybrid Nanostructures. *ACS Catal.* **2018**, *8* (4), 3602–3635. https://doi.org/10.1021/acscatal.8b00791.

(5) Fabian, D. M.; Hu, S.; Singh, N.; Houle, F. A.; Hisatomi, T.; Domen, K.; Osterloh, F. E.; Ardo, S. Particle Suspension Reactors and Materials for Solar-Driven Water Splitting. *Energy Environ. Sci.* **2015**, *8* (10), 2825–2850. https://doi.org/10.1039/C5EE01434D.

(6) Wu, H.-L.; Li, X.-B.; Tung, C.-H.; Wu, L.-Z. Semiconductor Quantum Dots: An Emerging Candidate for CO2 Photoreduction. *Adv. Mater.* **2019**, *31* (36), 1900709. https://doi.org/10.1002/adma.201900709.

(7) Yu, Y.; Ma, T.; Huang, H. Semiconducting Quantum Dots for Energy Conversion and Storage. *Adv. Funct. Mater.* **2023**, *33* (16), 2213770. https://doi.org/10.1002/adfm.202213770.

(8) Nagelj, N.; Brumberg, A.; Peifer, S.; Schaller, R. D.; Olshansky, J. H. Compositionally Tuning Electron Transfer from Photoexcited Core/Shell Quantum Dots via Cation Exchange. *J. Phys. Chem. Lett.* **2022**, *13* (14), 3209–3216. https://doi.org/10.1021/acs.jpclett.2c00333.

(9) Prusty, D.; Paramanik, L.; Parida, K. Recent Advances on Alloyed Quantum Dots for Photocatalytic Hydrogen Evolution: A Mini-Review. *Energy Fuels* **2021**, *35* (6), 4670–4686. https://doi.org/10.1021/acs.energyfuels.0c04163.

(10) Kameyama, T.; Takahashi, T.; Machida, T.; Kamiya, Y.; Yamamoto, T.; Kuwabata, S.; Torimoto, T. Controlling the Electronic Energy Structure of ZnS–AgInS2 Solid Solution Nanocrystals for Photoluminescence and Photocatalytic Hydrogen Evolution. *J. Phys. Chem. C* **2015**, *119* (44), 24740–24749. https://doi.org/10.1021/acs.jpcc.5b07994.

(11) Regulacio, M. D.; Han, M.-Y. Multinary I-III-VI 2and I 2-II-IV-VI 4Semiconductor Nanostructures for Photocatalytic Applications. *Acc. Chem. Res.* **2016**, *49* (3), 511–519.

(12) Murray, C. B.; Norris, D. J.; Bawendi, M. G. Synthesis and Characterization of Nearly Monodisperse CdE (E = Sulfur, Selenium, Tellurium) Semiconductor Nanocrystallites. *J. Am. Chem. Soc.* **1993**, *115* (19), 8706–8715. https://doi.org/10.1021/ja00072a025.

(13) Li, A.; Wang, T.; Li, C.; Huang, Z.; Luo, Z.; Gong, J. Adjusting the Reduction Potential of Electrons by Quantum Confinement for Selective Photoreduction of CO2 to Methanol. *Angew. Chem. Int. Ed.* **2019**, *58* (12), 3804–3808. https://doi.org/10.1002/anie.201812773.

(14) Tvrdy, K.; Frantsuzov, P. A.; Kamat, P. V. Photoinduced Electron Transfer from Semiconductor Quantum Dots to Metal Oxide Nanoparticles. *Proc. Natl. Acad. Sci.* **2011**, *108* (1), 29–34.

(15) Weiss, E. A. Designing the Surfaces of Semiconductor Quantum Dots for Colloidal Photocatalysis. *ACS Energy Lett.* **2017**, *2* (5), 1005–1013. https://doi.org/10.1021/acsenergylett.7b00061.

(16) Kodaimati, M. S.; McClelland, K. P.; He, C.; Lian, S.; Jiang, Y.; Zhang, Z.; Weiss, E. A. Viewpoint: Challenges in Colloidal Photocatalysis and Some Strategies for Addressing Them. *Inorg. Chem.* **2018**, *57* (7), 3659–3670. https://doi.org/10.1021/acs.inorgchem.7b03182.

(17) Harris, R. D.; Bettis Homan, S.; Kodaimati, M.; He, C.; Nepomnyashchii, A. B.; Swenson, N. K.; Lian, S.; Calzada, R.; Weiss, E. A. Electronic Processes within Quantum Dot-Molecule Complexes. *Chem. Rev.* **2016**, *116* (21), 12865–12919. https://doi.org/10.1021/acs.chemrev.6b00102.

(18) Burke, R.; Bren, K. L.; Krauss, T. D. Semiconductor Nanocrystal Photocatalysis for the Production of Solar Fuels. *J. Chem. Phys.* **2021**, *154* (3), 030901. https://doi.org/10.1063/5.0032172.
(19) Amirav, L.; Alivisatos, A. P. Photocatalytic Hydrogen Production with Tunable Nanorod Heterostructures. *J. Phys. Chem. Lett.* **2010**, *1* (7), 1051–1054. https://doi.org/10.1021/jz100075c.
(20) Zhu, H.; Song, N.; Lv, H.; Hill, C. L.; Lian, T. Near Unity Quantum Yield of Light-Driven Redox Mediator Reduction and Efficient H2 Generation Using Colloidal Nanorod Heterostructures. *J. Am. Chem. Soc.* **2012**, *134* (28), 11701–11708. https://doi.org/10.1021/ja303698e.
(21) Han, Z.; Qiu, F.; Eisenberg, R.; Holland, P. L.; Krauss, T. D. Robust Photogeneration of H2 in Water Using Semiconductor Nanocrystals and a Nickel Catalyst. *Science* **2012**, *338* (6112), 1321–1324. https://doi.org/10.1126/science.1227775.
(22) Wilker, M. B.; Utterback, J. K.; Greene, S.; Brown, K. A.; Mulder, D. W.; King, P. W.; Dukovic, G. Role of Surface-Capping Ligands in Photoexcited Electron Transfer between CdS Nanorods and [FeFe] Hydrogenase and the Subsequent H2 Generation. *J. Phys. Chem. C* **2018**, *122* (1), 741–750. https://doi.org/10.1021/acs.jpcc.7b07229.
(23) M. Chang, C.; L. Orchard, K.; M. Martindale, B. C.; Reisner, E. Ligand Removal from CdS Quantum Dots for Enhanced Photocatalytic H 2 Generation in pH Neutral Water. *J. Mater. Chem. A* **2016**, *4* (8), 2856–2862. https://doi.org/10.1039/C5TA04136H.
(24) Zhang, Z.; Edme, K.; Lian, S.; Weiss, E. A. Enhancing the Rate of Quantum-Dot-Photocatalyzed Carbon-Carbon Coupling by Tuning the Composition of the Dot's Ligand Shell. *J. Am. Chem. Soc.* **2017**, *139* (12), 4246–4249.
(25) Caputo, J. A.; Frenette, L. C.; Zhao, N.; Sowers, K. L.; Krauss, T. D.; Weix, D. J. General and Efficient C–C Bond Forming Photoredox Catalysis with Semiconductor Quantum Dots. *J. Am. Chem. Soc.* **2017**, *139* (12), 4250–4253. https://doi.org/10.1021/jacs.6b13379.
(26) Xin, Z.-K.; Huang, M.-Y.; Wang, Y.; Gao, Y.-J.; Guo, Q.; Li, X.-B.; Tung, C.-H.; Wu, L.-Z. Reductive Carbon–Carbon Coupling on Metal Sites Regulates Photocatalytic CO2 Reduction in Water Using ZnSe Quantum Dots. *Angew. Chem. Int. Ed.* **2022**, *61* (31), e202207222. https://doi.org/10.1002/anie.202207222.
(27) Chakraborty, I. N.; Roy, S.; Devatha, G.; Rao, A.; Pillai, P. P. InP/ZnS Quantum Dots as Efficient Visible-Light Photocatalysts for Redox and Carbon–Carbon Coupling Reactions. *Chem. Mater.* **2019**, *31* (7), 2258–2262. https://doi.org/10.1021/acs.chemmater.9b00086.
(28) Jiang, Y.; Wang, C.; Rogers, C. R.; Kodaimati, M. S.; Weiss, E. A. Regio- and Diastereoselective Intermolecular [2+2] Cycloadditions Photocatalysed by Quantum Dots. *Nat. Chem.* **2019**, *11* (11), 1034–1040. https://doi.org/10.1038/s41557-019-0344-4.
(29) Yuan, Y.; Jin, N.; Saghy, P.; Dube, L.; Zhu, H.; Chen, O. Quantum Dot Photocatalysts for Organic Transformations. *J. Phys. Chem. Lett.* **2021**, 7180–7193. https://doi.org/10.1021/acs.jpclett.1c01717.
(30) Brown, K. A.; Harris, D. F.; Wilker, M. B.; Rasmussen, A.; Khadka, N.; Hamby, H.; Keable, S.; Dukovic, G.; Peters, J. W.; Seefeldt, L. C.; King, P. W. Light-Driven Dinitrogen Reduction Catalyzed by a CdS:Nitrogenase MoFe Protein Biohybrid. *Science* **2016**, *352* (6284), 448–450. https://doi.org/10.1126/science.aaf2091.
(31) Ye, M.; Gao, X.; Hong, X.; Liu, Q.; He, C.; Liu, X.; Lin, C. Recent Advances in Quantum Dot-Sensitized Solar Cells: Insights into Photoanodes, Sensitizers, Electrolytes and Counter Electrodes. *Sustain. Energy Fuels* **2017**, *1* (6), 1217–1231. https://doi.org/10.1039/C7SE00137A.
(32) Nguyen, D.-T.; Chouat, A.; Do, T.-O. Highly Efficient Proton-Assisted Photocatalytic CO2 Reduction over 3-Mercaptopropionic Acid-Capped Quantums Dots. *Sustain. Energy Fuels* **2021**, *5* (16), 4015–4022. https://doi.org/10.1039/D1SE00641J.
(33) Bi, Q.-Q.; Wang, J.-W.; Lv, J.-X.; Wang, J.; Zhang, W.; Lu, T.-B. Selective Photocatalytic CO2 Reduction in Water by Electrostatic Assembly of CdS Nanocrystals with a Dinuclear Cobalt Catalyst. *ACS Catal.* **2018**, *8* (12), 11815–11821. https://doi.org/10.1021/acscatal.8b03457.

(34) Kuehnel, M. F.; Orchard, K. L.; Dalle, K. E.; Reisner, E. Selective Photocatalytic CO2 Reduction in Water through Anchoring of a Molecular Ni Catalyst on CdS Nanocrystals. *J. Am. Chem. Soc.* **2017**, *139* (21), 7217–7223. https://doi.org/10.1021/jacs.7b00369.
(35) Feng, Y.-X.; Wang, H.-J.; Wang, J.-W.; Zhang, W.; Zhang, M.; Lu, T.-B. Stand-Alone CdS Nanocrystals for Photocatalytic CO2 Reduction with High Efficiency and Selectivity. *ACS Appl. Mater. Interfaces* **2021**, *13* (22), 26573–26580. https://doi.org/10.1021/acsami.1c03606.
(36) Chaudhary, Y. S.; Woolerton, T. W.; Allen, C. S.; Warner, J. H.; Pierce, E.; Ragsdale, S. W.; Armstrong, F. A. Visible Light-Driven CO2 Reduction by Enzyme Coupled CdS Nanocrystals. *Chem. Commun.* **2011**, *48* (1), 58–60. https://doi.org/10.1039/C1CC16107E.
(37) Xin, Z.-K.; Gao, Y.-J.; Gao, Y.; Song, H.-W.; Zhao, J.; Fan, F.; Xia, A.-D.; Li, X.-B.; Tung, C.-H.; Wu, L.-Z. Rational Design of Dot-on-Rod Nano-Heterostructure for Photocatalytic CO2 Reduction: Pivotal Role of Hole Transfer and Utilization. *Adv. Mater.* **2022**, *34* (3), 2106662. https://doi.org/10.1002/adma.202106662.
(38) Sahm, C. D.; Ucoski, G. M.; Roy, S.; Reisner, E. Automated and Continuous-Flow Platform to Analyze Semiconductor–Metal Complex Hybrid Systems for Photocatalytic CO2 Reduction. *ACS Catal.* **2021**, *11* (17), 11266–11277. https://doi.org/10.1021/acscatal.1c02921.
(39) Sahm, C. D.; Mates-Torres, E.; Eliasson, N.; Sokołowski, K.; Wagner, A.; Dalle, K. E.; Huang, Z.; Scherman, O. A.; Hammarström, L.; García-Melchor, M.; Reisner, E. Imidazolium-Modification Enhances Photocatalytic CO2 Reduction on ZnSe Quantum Dots. *Chem. Sci.* **2021**, *12* (26), 9078–9087. https://doi.org/10.1039/D1SC01310F.
(40) Sahm, C. D.; Ciotti, A.; Mates-Torres, E.; Badiani, V.; Sokołowski, K.; Neri, G.; Cowan, A. J.; García-Melchor, M.; Reisner, E. Tuning the Local Chemical Environment of ZnSe Quantum Dots with Dithiols towards Photocatalytic CO2 Reduction. *Chem. Sci.* **2022**, *13* (20), 5988–5998. https://doi.org/10.1039/D2SC00890D.
(41) Kuehnel, M. F.; Sahm, C. D.; Neri, G.; Lee, J. R.; Orchard, K. L.; Cowan, A. J.; Reisner, E. ZnSe Quantum Dots Modified with a Ni(Cyclam) Catalyst for Efficient Visible-Light Driven CO2 Reduction in Water. *Chem. Sci.* **2018**, *9* (9), 2501–2509. https://doi.org/10.1039/C7SC04429A.
(42) Arcudi, F.; Đorđević, L.; Nagasing, B.; Stupp, S. I.; Weiss, E. A. Quantum Dot-Sensitized Photoreduction of CO2 in Water with Turnover Number > 80,000. *J. Am. Chem. Soc.* **2021**, *143* (43), 18131–18138. https://doi.org/10.1021/jacs.1c06961.
(43) Lian, S.; Kodaimati, M. S.; Weiss, E. A. Photocatalytically Active Superstructures of Quantum Dots and Iron Porphyrins for Reduction of CO2 to CO in Water. *ACS Nano* **2018**, *12* (1), 568–575. https://doi.org/10.1021/acsnano.7b07377.
(44) Huang, J.; Xu, B.; Tian, L.; Pati, P. B.; Etman, A. S.; Sun, J.; Hammarström, L.; Tian, H. A Heavy Metal-Free CuInS2 Quantum Dot Sensitized NiO Photocathode with a Re Molecular Catalyst for Photoelectrochemical CO2 Reduction. *Chem. Commun.* **2019**, *55* (55), 7918–7921. https://doi.org/10.1039/C9CC04222A.
(45) Huang, J.; Gatty, M. G.; Xu, B.; Pati, P. B.; Etman, A. S.; Tian, L.; Sun, J.; Hammarström, L.; Tian, H. Covalently Linking CuInS2 Quantum Dots with a Re Catalyst by Click Reaction for Photocatalytic CO2 Reduction. *Dalton Trans.* **2018**, *47* (31), 10775–10783. https://doi.org/10.1039/C8DT01631C.
(46) Zhang, J.; Bifulco, A.; Amato, P.; Imparato, C.; Qi, K. Copper Indium Sulfide Quantum Dots in Photocatalysis. *J. Colloid Interface Sci.* **2023**, *638*, 193–219. https://doi.org/10.1016/j.jcis.2023.01.107.
(47) Chen, S.; Yin, H.; Liu, P.; Wang, Y.; Zhao, H. Stabilization and Performance Enhancement Strategies for Halide Perovskite Photocatalysts. *Adv. Mater.* **2023**, *35* (6), 2203836. https://doi.org/10.1002/adma.202203836.
(48) Wang, J.; Shi, Y.; Wang, Y.; Li, Z. Rational Design of Metal Halide Perovskite Nanocrystals for Photocatalytic CO2 Reduction: Recent Advances, Challenges, and Prospects. *ACS Energy Lett.* **2022**, *7* (6), 2043–2059. https://doi.org/10.1021/acsenergylett.2c00752.

(49) Banski, M.; Afzaal, M.; Malik, M. A.; Podhorodecki, A.; Misiewicz, J.; O'Brien, P. Special Role for Zinc Stearate and Octadecene in the Synthesis of Luminescent ZnSe Nanocrystals. *Chem. Mater.* **2015**, *27* (11), 3797–3800. https://doi.org/10.1021/acs.chemmater.5b00347.
(50) Toufanian, R.; Zhong, X.; Kays, J. C.; Saeboe, A. M.; Dennis, A. M. Correlating ZnSe Quantum Dot Absorption with Particle Size and Concentration. *Chem. Mater.* **2021**, *33* (18), 7527–7536. https://doi.org/10.1021/acs.chemmater.1c02501.
(51) Morris, A. J.; Meyer, G. J.; Fujita, E. Molecular Approaches to the Photocatalytic Reduction of Carbon Dioxide for Solar Fuels. *Acc. Chem. Res.* **2009**, *42* (12), 1983–1994. https://doi.org/10.1021/ar9001679.
(52) Takeda, H.; Cometto, C.; Ishitani, O.; Robert, M. Electrons, Photons, Protons and Earth-Abundant Metal Complexes for Molecular Catalysis of CO2 Reduction. *ACS Catal.* **2017**, *7* (1), 70–88. https://doi.org/10.1021/acscatal.6b02181.
(53) Call, A.; Cibian, M.; Yamamoto, K.; Nakazono, T.; Yamauchi, K.; Sakai, K. Highly Efficient and Selective Photocatalytic CO2 Reduction to CO in Water by a Cobalt Porphyrin Molecular Catalyst. *ACS Catal.* **2019**, *9* (6), 4867–4874. https://doi.org/10.1021/acscatal.8b04975.
(54) Knauf, R. R.; Lennox, J. C.; Dempsey, J. L. Quantifying Ligand Exchange Reactions at CdSe Nanocrystal Surfaces. *Chem. Mater.* **2016**, *28* (13), 4762–4770. https://doi.org/10.1021/acs.chemmater.6b01827.
(55) Nakazono, T.; Parent, A. R.; Sakai, K. Cobalt Porphyrins as Homogeneous Catalysts for Water Oxidation. *Chem. Commun.* **2013**, *49* (56), 6325–6327. https://doi.org/10.1039/C3CC43031F.
(56) Matsui, T.; Kitagawa, Y.; Okumura, M.; Shigeta, Y. Accurate Standard Hydrogen Electrode Potential and Applications to the Redox Potentials of Vitamin C and NAD/NADH. *J. Phys. Chem. A* **2015**, *119* (2), 369–376. https://doi.org/10.1021/jp508308y.
(57) Sampaio, R. N.; Grills, D. C.; Polyansky, D. E.; Szalda, D. J.; Fujita, E. Unexpected Roles of Triethanolamine in the Photochemical Reduction of CO2 to Formate by Ruthenium Complexes. *J. Am. Chem. Soc.* **2020**, *142* (5), 2413–2428. https://doi.org/10.1021/jacs.9b11897.
(58) Zhu, H.; Yang, Y.; Wu, K.; Lian, T. Charge Transfer Dynamics from Photoexcited Semiconductor Quantum Dots. *Annu. Rev. Phys. Chem.* **2016**, *67* (1), 259–281. https://doi.org/10.1146/annurev-physchem-040215-112128.
(59) Fernández-Terán, R. J.; Sucre-Rosales, E.; Echevarria, L.; Hernández, F. E. A Sweet Introduction to the Mathematical Analysis of Time-Resolved Spectra and Complex Kinetic Mechanisms: The Chameleon Reaction Revisited. *J. Chem. Educ.* **2022**, *99* (6), 2327–2337. https://doi.org/10.1021/acs.jchemed.2c00104.
(60) Watson, K. M.; Asbury, J. B. Synthesis and Photoinduced Electron Transfer Studies of Ligand Exchanged Mn-Doped ZnSe Nanocrystals in Water. *J. Phys. Chem. C* **2022**. https://doi.org/10.1021/acs.jpcc.2c00379.